



ELSEVIER

Available online at www.sciencedirect.com

SCIENCE @ DIRECT®

Earth and Planetary Science Letters 216 (2003) 565–574

EPSL

www.elsevier.com/locate/epsl

Fluxes of fluid and heat from the oceanic crustal reservoir

H. Paul Johnson*, Matthew J. Pruis

School of Oceanography, University of Washington, Seattle, WA 98195-7940, USA

Received 10 March 2003; received in revised form 3 September 2003; accepted 19 September 2003

Abstract

Recent discoveries define a global scale fluid reservoir residing within the uppermost igneous oceanic crust, a region of seafloor that is both warm and may harbor a substantial biosphere. This hydrothermal fluid reservoir formed initially within volcanic rocks newly erupted at mid-ocean ridges, but extends to the vastly larger and older ridge flanks. Upper oceanic crust is porous and permeable due to the presence of lava drainbacks, fissuring, and inter-unit voids, and this porosity and permeability allows active fluid circulation to advect measurable quantities of lithospheric heat from the crust to an average age of 65 Myr. A compilation of crustal porosities shows that this fluid reservoir contains nearly 2% of the total volume of global seawater. Heat flow and sediment thickness data allow calculation of reservoir temperatures, predicting 40°C mean temperatures in Cretaceous crust. Utilizing these temperature estimates, heat flow measurements and models for the thermal structure and evolution of the oceanic lithosphere, we have computed mean hydrothermal fluxes into the deep ocean as a function of plate age. The total hydrothermal volume flux into the oceans approaches 20% of the total riverine input and may contribute to the global seawater mass balance.

© 2003 Elsevier B.V. All rights reserved.

Keywords: ocean crustal reservoir; hydrothermal circulation; heat flux; crustal porosity

1. The oceanic crustal reservoir

Porosities of upper oceanic crust can be derived from seafloor gravity measurement [1], the down-hole logging of drill holes [2–5], and geological studies of terrestrially exposed ophiolites [6]. Crustal porosities younger than 10 Myr [1] and published values for older crust are compiled in Table 1 and shown in Fig. 1, demonstrating the non-uniform age distribution of these data. Crus-

tal porosity values within the neo-volcanic zone can approach 34% soon after formation, decreasing to 15% in less than 1 Myr [1]. Although older seafloor measurements are sparse, no strong age-dependent decrease in crustal porosity after 10 Myr is apparent in the data. If this interpretation of very limited data is globally representative, average porosity for the entire upper crust can be obtained by integrating over the amount of seafloor present for each age interval, giving an average for oceanic upper crustal porosity of 12%. While this is a surprisingly large volume, solid mini-cores of intact rock taken from DSDP/ODP drill holes have a measured, and therefore connected, porosity in excess of 6% for crust of

* Corresponding author. Fax: +1-206-543-0275.

E-mail address: johnson@ocean.washington.edu
(H.P. Johnson).

Table 1
Data for the determination of upper crustal porosity

Location	Latitude	Longitude	ρ_c	\pm	Φ_m (%)	\pm	Φ_c (%)	Age (Ma)	Reference
Gorda	42°41'	−126°47'	2270	260	34	16	35	0.00	[1]
CoAxial	46°32'	−126°35'	2450	110	29	6	25	0.00	[29]
CoAxial	46°32'	−126°34'	2330	100	31	5	32	0.00	[29]
CoAxial	46°19'	−129°43'	2280	50	36	3	34	0.00	[29]
CoAxial	46°32'	−129°34'	2810	150	9	8	6	0.01	[29]
CoAxial	46°30'	−129°36'	2470	160	26	7	24	0.01	[29]
CoAxial	46°29'	−129°36'	2430	180	28	10	26	0.01	[29]
CoAxial	46°19'	−129°42'	2770	60	10	4	8	0.01	[29]
Endeavour	47°57'	−129°6'	2240	50	38	4	36	0.01	[30]
EPR	21°00'	−109°	2620	90	15	5	16	0.03	[31]
Endeavour	47°58'	−129°05'	2520		23		22	0.05	[10]
EPR	9°50'	−104°14'	2410				27	0.08	[32]
WMARK	23°50'	−46°18'	2784	78			8	0.1	[33]
Axial	45°58'	−130°02'	2230	80			37	0.1	[34]
EPR	9°31'	−104°17'	2690				13	0.2	[32]
Middle Valley	49°27'	−128°42'	2630				16	0.2	[35]
TAG	26°08'	−44°49'	2400	100	25	5	28	0.2	[36]
Endeavour	48°00'	−129°11'	2770		10		8	0.2	[10]
EPR	9°48'	−104°12'	2420	80			27	0.4	[37]
Endeavour	48°00'	−129°16'	2710		13		12	0.4	[10]
Endeavour	48°00'	−129°19'	2750		11		9	0.6	[10]
Cleft	44°52'	−130°15'	2630	50			16	0.7	[38]
Endeavour	48°03'	−129°22'	2750		11		9	0.7	[10]
Blanco	44°25'	−130°10'	2530	120	23	10	21	1	[12]
WMARK	23°56'	−46°02'	2658				14	2	[33]
504B ^a	1°14'	−83°44'	2700		10	3	12	6	[2]
395A ^a	22°45'	−46°05'	2690				13	7	[4]
396B ^a	22°59'	−43°31'	2600		17		17	10	[39,46]
Troodos ^b	35°20'	33°25'					9	90	[6]
Erimo Smt	41°00'	145°00'	2700				12	104	[40]
843 ^a	19°21'	−159°06'	2700				12	110	[41]
417D ^a	25°07'	−68°03'	2680		12		13	118	[42]
418A ^a	25°02'	−68°03'	2660		13		14	118	[3]
801C ^a	18°39'	156°22'	2750				9	157	[43]

ρ_c = measured crustal density from ocean bottom gravity measurements or gamma density in case of borehole data.

Φ_m = measured porosity of site (when grain density determined from local rock samples).

Φ_c = estimated porosity assuming grain density of 2930 kg/m³ and water density of 1030 kg/m³.

^a This value is from a drill hole and not obtained from ocean bottom gravity measurements.

^b This value is from a geological study of an ophiolite.

ridge flank ages [7]. Since recovered DSDP/ODP drill cores represent only the most continuous and robust portions of the solid matrix of upper oceanic crust, an additional 6% porosity present as larger-scale voids, drainbacks, breccia zones and inter-flow cavities, which are not recovered during drilling, is plausible.

Calculation of reservoir volume also requires estimates of the vertical dimension. Accepting the equivalence between high porosity upper crust

and seismic layer 2A [8,9] could both provide this estimate and extend the limited number of direct measurements of upper crustal thickness globally [2–5,10,11]. Seismic models give two bounding models for upper crustal thickness: (a) 600 m of constant porosity [9] and (b) an upper 300 m of constant porosity, plus a linearly decreasing porosity for the lower 300 m [10]. These bounds give estimates for the total free water within upper oceanic crustal rocks of: (a) 26×10^6 km³ and

Table 2
Parameters used in determining the physical properties of the crustal reservoir

Age bins (Ma)	Porosity of upper extrusives	Sediment thickness	Heat flow	Heat flow (GDH-1)	Sediment thermal conductivity	Top of upper extrusives temperature	Upper extrusives thermal conductivity	Bottom of upper extrusives temperature	Hydrothermal volume flux	Residence time												
(min)	(max)	(m)	(mW/m ²)	(mW/m ²)	(W/m ² K)	(°C)	(W/m ² K)	(°C)	(km ³ /yr)	(years)												
0.0	1.0	0.5	0.21	0.12	0.02	167	86	59	9	101	1.12	0.35	10	5	2.18	7	492	7	505	323	1860	
0.0	4.8	2.4	0.20	0.14	0.02	186	96	55	8	93	1.13	0.35	11	6	2.18	6	2.18	7	430	281	2190	
0.0	4.8	9.7	7.2	0.14	0.03	95	55	110	11	464	1.07	0.35	10	7	2.02	7	2.02	18	3037	2307	540	
9.7	14.1	11.9	0.12	0.02	124	74	109	11	149	1.10	0.35	14	6	2.18	6	2.18	12	337	248	2800		
14.1	18.9	16.5	0.12	0.02	127	75	77	9	126	1.11	0.35	10	6	2.18	6	2.18	12	337	248	2800		
18.9	23.4	21.2	0.12	0.02	150	78	67	7	111	1.12	0.35	11	6	2.18	6	2.18	7	505	323	1860		
23.4	28.0	25.7	0.12	0.02	167	86	59	9	101	1.12	0.35	10	5	2.18	5	2.18	7	492	325	1910		
28.0	32.6	30.3	0.12	0.02	186	96	55	8	93	1.13	0.35	11	6	2.18	6	2.18	7	430	281	2190		
32.6	38.5	35.5	0.12	0.02	205	109	50	9	86	1.14	0.35	11	6	2.18	6	2.18	7	403	275	2340		
38.5	45.3	41.9	0.12	0.02	208	109	62	8	79	1.14	0.35	13	7	2.18	7	2.18	30	155	123	6050		
45.3	51.8	48.6	0.12	0.02	228	128	63	7	73	1.15	0.35	14	8	2.18	8	2.18	9	87	83	10800		
51.8	58.6	55.2	0.12	0.02	259	158	58	6	69	1.16	0.35	14	9	2.18	9	2.18	10	85	76	11000		
58.6	66.4	62.3	0.12	0.02	307	203	57	7	65	1.18	0.36	16	11	2.18	11	2.18	12	54	63	17000		
66.4	74.2	70.3	0.12	0.02	364	255	60	5	62	1.21	0.36	20	14	2.18	14	2.18	14	11	29	80000		
74.2	82.3	78.2	0.12	0.02	435	307	61	7	59	1.24	0.37	23	17	2.18	17	2.18	17	-9	20	24	-	
82.3	91.7	87.0	0.12	0.02	564	366	52	4	57	1.29	0.38	24	16	2.18	16	2.18	17	20	0.03	24	-	
91.7	103.4	97.5	0.12	0.02	673	477	52	5	54	1.34	0.40	28	20	2.18	20	2.18	21	10	0.03	21	-	
103.4	114.0	108.7	0.12	0.02	633	501	54	3	53	1.32	0.40	27	22	2.18	22	2.18	22	-5	14	-	-	
114.0	129.9	122.0	0.12	0.02	783	591	51	2	51	1.38	0.43	31	24	2.18	24	2.18	24	0	0.03	24	-	-
129.9	148.3	139.1	0.12	0.02	614	394	47	3	50	1.31	0.38	24	16	2.18	16	2.18	16	13	18	18	-	-
148.3	179.8	164.0	0.12	0.02	1013	882	43	4	49	1.48	0.51	31	27	2.18	27	2.18	28	23	25	25	-	-

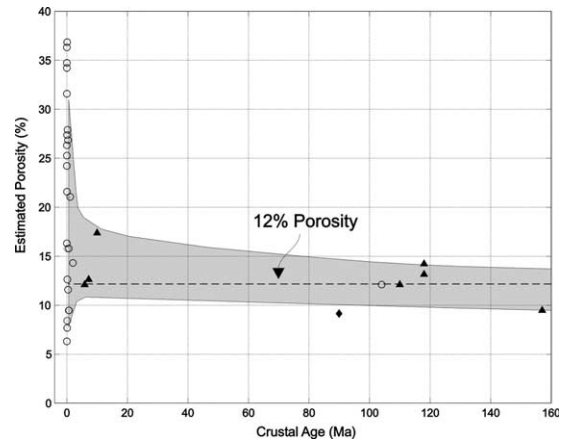


Fig. 1. Porosity of upper oceanic crust as a function of age. The high variability in young crust is due to structural differences between low density pillowed units with abundant voids and high density massive flows. This variability decreases with age, with the collapse of large voids and the fracturing of massive units as crust is transported out of the neo-volcanic zone. Open circles, ocean bottom gravity measurements. Filled triangles, downhole logging of drill holes. Filled diamond is an ophiolite study [6].

(b) $19 \times 10^6 \text{ km}^3$, with the larger value being supported by seafloor gravity studies [12] and used in our calculations. Error estimates for reservoir volume represent $\pm 150 \text{ m}$ uncertainty in the 600 m layer thickness and the computed uncertainty in porosity (Table 2). Low values for uncertainty in porosity of older crust are likely due to the under-sampling of these regions.

2. Properties of the crustal reservoir

Average thermal characteristics of the global crustal reservoir can be estimated by merging heat flow and sediment thickness data determined over wide geographical areas into a single ‘box’ model of the seafloor and using crustal age as the common index (Table 2). While useful for estimating global properties when data are sparse [13,14], this model is unlikely to successfully predict crustal properties at any given geographical location. Uncertainties for all crustal properties were estimated by iteratively removing samples greater than 5 standard deviations from the mean, and then computing the remaining average

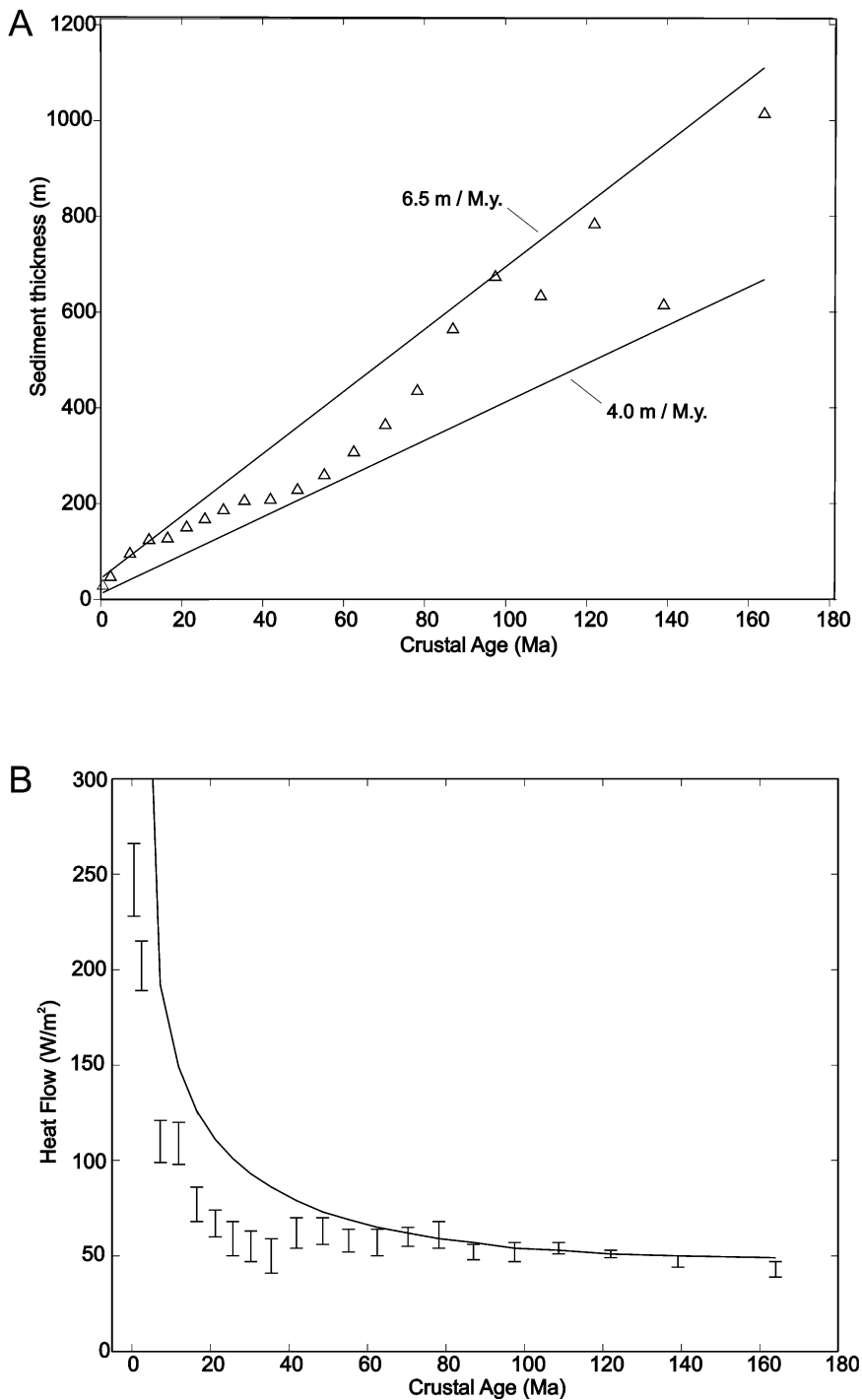


Fig. 2. (A) Global sediment thickness as a function of crustal age. The geographically distributed data [15] are merged with crustal age [16] and then compiled in 20 equal area bins. Dashed bounding lines represent global sedimentation rates of 6.5 and 4.0 m/Myr respectively. (B) Compiled global heat flow data [17] compared to predicted flux from the purely conductive GDH-1 model [13,14]. The difference between measured heat flow and the conductive model represents two-way advection of heat and fluid between the crustal reservoir and overlying seawater.

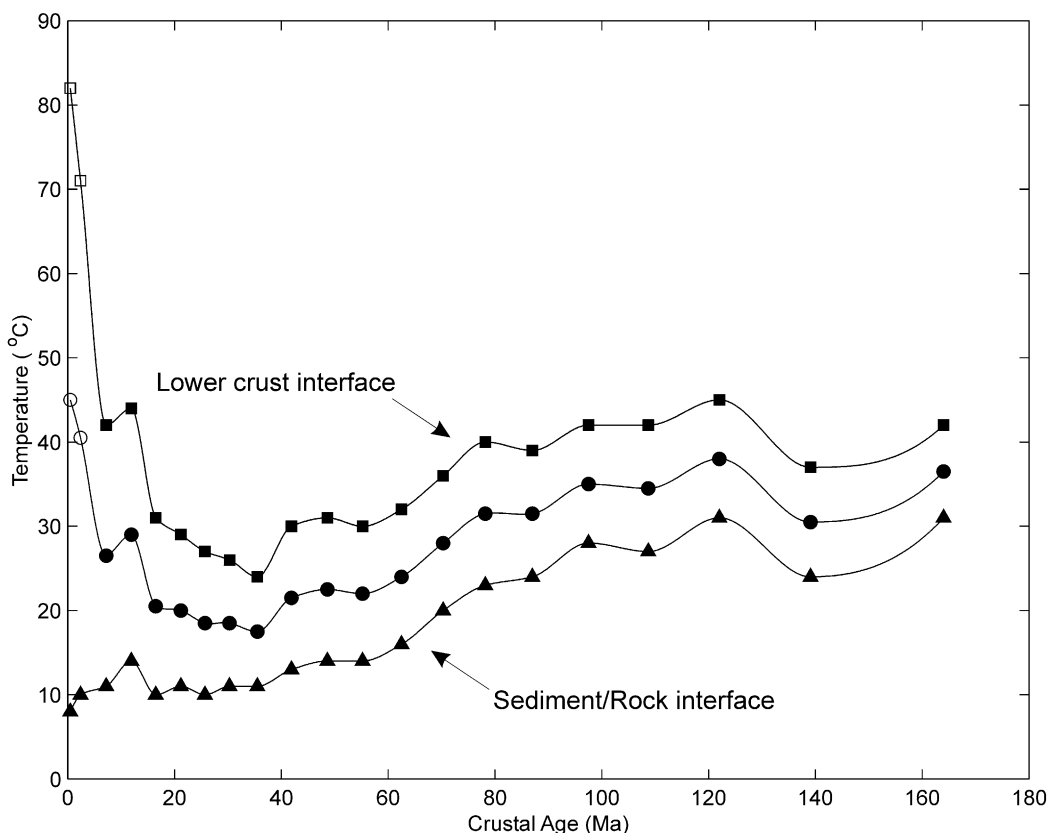


Fig. 3. Estimated temperatures for the crustal reservoir as a function of age. Triangles are temperatures for the sediment/rock interface, squares are values for the bottom of the 600 m thick high porosity zone, and circles are the mean for the entire upper crustal reservoir. Open symbols have higher uncertainty ($>20\%$) due to the assumption of no fluid convection within the crustal section. Temperatures represented as filled symbols should be independent of this assumption.

deviation. Twenty equal area age bins, each 5% of the total range, were chosen for all distributions other than porosity. An additional age bin of 0–1 Ma crust allowed identification of young on-axis hydrothermal flux, and each subsequent bin contains an area of $1.34 \times 10^4 \text{ km}^2$. Global sediment thickness for the ocean basins has been determined geographically [15] and then merged with a separate crustal age distribution [16]. These data do not include Atlantic data north of 50°N [15]. Sediment thickness for time intervals of equal area are plotted as a function of age in Fig. 2, showing the expected systematic increase in sediment cover with increasing crustal age.

Heat flow data were also compiled geographically [17], marginal basins were excluded, and then merged with crustal age over the same inter-

vals as in Fig. 2. Although Fig. 3 represents more heat flow data than used by the most recent previous compilation [13,14], our results are not dramatically different. The age of 65 Myr where heat flow data and the conductive flux model merge, and where the crustal reservoir can be considered convectively disconnected from the overlying ocean by thick impermeable sediments, is approximately the same as that determined by previous analyses [13]. This is a globally averaged crustal age, and both venting and re-charge of fluid can occur locally in much older crust [14].

3. Crustal temperatures

Biological and chemical processes within the

oceanic crustal reservoir depend strongly on temperature. To estimate the temperature variation of the sediment/basement interface with crustal age, we used a method previously applied to heat flow data on the eastern flank of the Juan de Fuca Ridge, which was verified by the logging of several ODP holes [18]. In this technique, temperature gradients determined from surficial heat flow measurements are projected downward to the sediment/basement interface, using estimates of sediment thickness and thermal conductivity, and adjusted for bottom water temperature. Sediment thermal conductivities can vary both geographically and as a function of depth, and we used a global compilation derived from the extensive ODP data set [19]. The linear fit applied to sediment thermal conductivity (T_c) data as a function of depth is:

$$T_c = 8.4312 \times 10^{-4} \times (\text{sediment thickness})/2 + 1.0525 \quad (1)$$

with an uncertainty for each point of ± 0.35 W/m/°K. Basement temperatures at the sediment/rock interface were calculated using $Q = C \partial T / \partial z$, where Q is heat flow in W/m², C is thermal conductivity in W/m/°K, T is temperature in °K, and z is vertical dimension in meters. Results from the calculation of sediment/basement interface temperatures are shown in Fig. 3, with the youngest (sediment-covered) basement temperatures near 10°C, rising near 30°C for 120 Myr old crust.

Estimates of reservoir temperatures below the upper sediment/basalt interface require projection of the heat flow-derived thermal gradient into a porous medium that may contain convecting fluid and therefore may not be well-represented by heat conduction in a solid. Any vertical fluid motion occurring within the reservoir will increase effective

thermal conductivity, resulting in lower crustal temperatures for the same heat flow than for a non-convecting environment [20,21]. If, however, the vertical fluid velocity of this convection is slow (tens of cm/yr [22]), vertical temperature gradients within igneous basement can be approximated as a non-convecting mixture of water and rock. This assumption allows the effective thermal conductivity to be estimated using a simple mixing model based on crustal porosity and the static physical properties of the two phases. Crustal permeabilities in youngest ocean crust appear larger than the critical value for the onset of fluid convection [23]. However, in basement older than 4 Myr, any perturbation to conductive thermal gradients by convection becomes small due to the reduction in crustal permeability by three orders of magnitude [20,21]. For these calculations, effective thermal conductivities for within the upper extrusive layer were determined using a mixing model between basalt of 2.4 W/m/°K and seawater of 0.528 W/m/°K calculated as:

$$T_c = 2.4 \times (1 - \Phi) + 0.528 \times \Phi \quad (2)$$

where Φ is crustal porosity from our Fig. 1.

In order to test the use of the simple mixing model for crustal thermal conductivities, heat flow values for several ODP drill sites were projected downward into the crust below the basement/sediment interface (Table 3). The temperature gradient of the crustal section was measured during the downhole logging of each hole and compared to the temperature gradient predicted using the simple mixing model for crustal thermal conductivity. In the three cases below, temperature gradients were measured long after the cessation of the drilling, and, for Hole 504b, after fluid exchange through the drill hole had largely ceased. For Hole 504b, only the temperature gra-

Table 3
Test of the mixing model for crustal thermal conductivity

Drill hole	Crustal age (Myr)	Sediment thickness (m)	Basalt penetrated (m)	Porosity	Heat flow (W/m ²)	Temperature gradient measured (°C/m)	Temperature gradient predicted (°C/m)	Reference
843b	110	242	71	12	0.051	0.0258	0.0235	[44]
417D	106	343	366	12	0.0462	0.022	0.212	[42]
504b	5.9	274	1300	11	0.196	0.091	0.116	[45]

dient in the upper 600 m of basement was included in the average. Active fluid circulation would increase the effective thermal conductivity, and reduce the measured temperature gradient, by 20% in the case of 504B. Our interpretation of these results is that conduction in a porous solid is a reasonable approximation for crustal heat transfer, particularly in crust older than 4 Myr.

Estimated mean basement temperatures using this simple non-convecting model are substantially elevated above bottom water temperatures, increasing to near 40°C in crust of mid-Cretaceous age (Fig. 3). This increase of crustal temperature with increasing age older than 20 Myr is a consequence of a relatively uniform heat flow for older crust that is accompanied by an increase in Cretaceous sediment thickness (Fig. 2). Although the middle and lower reservoir temperatures can be over-estimated by this method by as much as 20% in young crust where convection is present [20,21], the temperatures at the sediment/rock interface, and the associated thermal and fluid

fluxes into the ocean, are not affected by the model assumptions.

4. Thermal flux

For a given age interval, the difference between measured heat flow and the thermal flux expected for a conductive-only plate model provides an estimate of the ‘missing’ heat flux due to the advection of fluid from basement to overlying seawater [13,14]. These differences between measurement and model, along with sediment/basement temperatures (Fig. 3) and a global bottom water temperature of $1.5 \pm 0.5^\circ\text{C}$ [24], were converted into estimates of fluid flux into/out of the basement reservoir as a function of crustal age (Fig. 4). Volume fluxes were determined using:

$$Q_h = \rho Cq(T - T_o) / A \tag{3}$$

where Q_h is the heat flux, ρ = water density, C is the specific heat of water, q is the volume flux, T is temperature at the rock/sediment interface, T_o

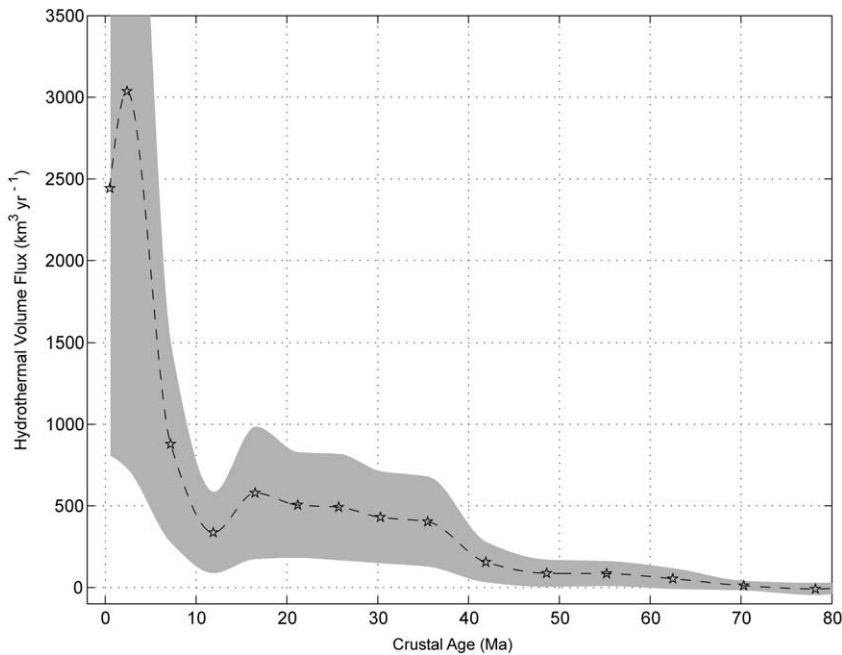


Fig. 4. Flux of hydrothermal fluid to/from the crustal reservoir as a function of age. Shaded area shows the range of propagated uncertainties that contain 50% of the calculated values for each age bin. Estimates of flux are high for young crust and approach zero at 65 Myr.

is the bottom water temperature and A is the area of the seafloor in the bin. Other parameter uncertainties were propagated to obtain the uncertainty in volume flux.

As measured heat flow data approach purely conductive values (Fig. 2B), average fluid flux approaches zero for crust 65 Myr and older. Fig. 4 shows that at least 50% of the total global hydrothermal flux is from ridge flank crust with ages between 4 Myr and 65 Myr. Our analysis does not include the small component of high temperature venting from the axial zone where fluid temperatures can exceed 350°C [25], which would require the percentage of the off-axis fluid flux to be slightly larger. Residence times were calculated using the volume of each bin divided by the flux for that bin. For the hydrothermal fluid within the global upper crustal reservoir, this residence time is $(1.95 \times 10^{16} \text{ m}^3)/(7.1 \times 10^{12} \text{ m}^3/\text{yr})$, or approximately 2700 years.

5. Discussion

Recent global data compilations permit first-order estimates of the size and basic physical properties of an unexpectedly large reservoir of seawater residing within upper oceanic crust. Crustal porosity data indicate that the reservoir contains $2 \times 10^7 \text{ km}^3$ of fluid, a quantity that is approximately 40% the volume of the Arctic Ocean and four times the combined Mediterranean and Black seas. Mean crustal temperatures decrease from 40°C for the youngest ages through a minimum at 20 Myr, then increase to near 50°C for the oldest seafloor. It is probably significant in terms of an oceanic crustal biosphere that global average reservoir temperatures everywhere are below the proposed 113°C upper limit on microbial activity [26]. Our analysis agrees with earlier compilations using fewer data [13,14,25] that show general isolation of the crustal reservoir from overlying seawater occurs near 65 Myr. Calculations based on these parameters give a total age-integrated flux of $7.1 \times 10^{12} \text{ m}^3/\text{yr}$ of hydrothermal fluid, with $2.3 \times 10^{12} \text{ m}^3/\text{yr}$ in the axial region and $4.8 \times 10^{12} \text{ m}^3/\text{yr}$ occurring in crust older than between 5 Myr and 65 Myr. These compare to

previous estimates of $4.2 \times 10^{12} \text{ m}^3/\text{yr}$ (axial flux [25]), $7.3 \times 10^{12} \text{ m}^3/\text{yr}$ (flank flux [25]) and $11.5 \times 10^{12} \text{ m}^3/\text{yr}$ (total flux [25]) and $2.5 \times 10^{12} \text{ m}^3/\text{yr}$ (flank flux only [22]) that were based on earlier data compilations.

While our estimated global hydrothermal fluid flux amounts to 18% of that due to riverine flow into the oceans, which is assumed to be $4 \times 10^{13} \text{ m}^3/\text{yr}$ [27], the impact of this flux on the seawater chemical inventory is uncertain. The composition of hydrothermal fluid from varying reservoir source temperatures is substantially different than river water, and crustal fluid is injected near the seafloor while river input is added at or near the surface. There is a continuing ambiguity in the chemical composition of the ridge flank hydrothermal fluid, which is strongly dependent on temperature, age, rock alteration and circulation history, and only limited fluid chemical analyses are available from anomalous sites unlikely to represent global averages [22,25,28].

With our calculated flux rates and reservoir size, an integrated mean residence time for fluid within the crustal reservoir can be estimated as 2700 yr, although for heavily sedimented crust older than 65 Myr, residence times for these isolated sections can approach very long periods. Similar calculations show that the net global flux rate would circulate the entire volume of seawater through the upper ocean crust in only 200 000 yr, significantly shorter than previous estimates [25]. If, however, a major portion of the crustal porosity is isolated from the general hydrothermal circulation by sediment cover, rock alteration or chemical precipitation, the total effective reservoir size will be smaller, and the calculated residence and ocean through-put times will also be shortened. While our analysis is based on an extrapolation of geographically limited data, hydrothermal fluid contained within the upper oceanic crustal rocks appears to form an unexplored body of seawater that is truly global in scale.

Acknowledgements

This research was supported by NSF Grants

OCE9911523 and OCE0085615 to H.P.J. A. Fisher contributed an insightful review. **[BOYLE]**

References

- [1] M.J. Pruis, H.P. Johnson, Age dependent porosity of young upper oceanic crust: Insights from seafloor gravity studies of recent volcanic eruptions, *Geophys. Res. Lett.* 29 (2002) 20.1–20.4.
- [2] J.R. Cann, R.P. Von Herzen, Downhole logging at deep sea drilling project sites 501, 504, and 505, near the Costa Rica Rift, *Init. Rep. DSDP 69* (1984) 281–299.
- [3] R.L. Carlson, K.R. Snow, R.H. Wilkens, Density of old oceanic crust: An estimate derived from downhole logging on ODP leg 102, *Proc. ODP Sci. Results 102* (1988) 63–68.
- [4] M. Mathews, M.H. Salisbury, R. Hyndman, Basement logging on the Mid-Atlantic Ridge, Deep Sea Drilling Project hole 395A, *Init. Rep. DSDP 78B* (1983) 717–730.
- [5] D. Moos, M. Van Schaack, H. Ito, Elastic-wave velocities in Jurassic-age oceanic crust from analysis of sonic full waveform logs in Hole 801C, *Proc. ODP Sci. Results 144* (1995) 665–671.
- [6] K.M. Gillis, K. Sapp, Distribution of porosity in a section of upper oceanic crust exposed in the Troodos Ophiolite, *J. Geophys. Res.* 102 (B5) (1997) 10133–10149.
- [7] H.P. Johnson, S.W. Semyan, Time variation of the physical properties of oceanic basalts: Implications for crustal formation and evolution, *J. Geophys. Res.* 99 (1994) 3123–3135.
- [8] R.L. Carlson, C.N. Herrick, Densities and porosities in the oceanic crust and their variations with depth and age, *J. Geophys. Res.* 95 (1990) 9153–9170.
- [9] E. Morris, R.S. Detrick, T.A. Minshull, J.C. Mutter, R. White, W. Su, P. Buhl, Seismic structure of oceanic crust in the western North Atlantic, *J. Geophys. Res.* 98 (B8) (1993) 13879–13903.
- [10] E.E. Hooft, H. Shouten, R.S. Detrick, Constraining crustal emplacement processes from the variation in seismic Layer 2A thickness at the East Pacific Rise, *Earth Planet. Sci. Lett.* 142 (1996) 289–309.
- [11] M.L. Holmes, H.P. Johnson, Upper crustal densities derived from sea floor gravity measurements: Northern Juan de Fuca Ridge, *Geophys. Res. Lett.* 20 (1993) 1871–1874.
- [12] H.P. Johnson, M.J. Pruis, D. Van Patten, M.A. Tivey, Density and porosity of upper oceanic crust from seafloor gravity measurements, *Geophys. Res. Lett.* 27 (2000) 1053–1056.
- [13] C.S. Stein, S. Stein, A model for the global variation in oceanic depth and heat flow with lithospheric age, *Nature* 359 (1992) 123–129.
- [14] C.S. Stein, S. Stein, Constraints on hydrothermal heat flux through the oceanic lithosphere from global heat flow, *J. Geophys. Res.* 99 (1994) 3081–3095.
- [15] D. Divens, Total sediment thickness of the world's oceans, National Oceanic and Atmospheric Administration, US Department of Commerce, Boulder, CO, 1996 [available on the Web at <http://www.ngdc.noaa.gov/mgg/sedthick/sedthick.html>].
- [16] R.D. Mueller, W.R. Roest, J.-Y. Royer, L.M. Gahagan, J.G. Sclater, A digital age map of the ocean floor, SIO Reference Series 93-30, Scripps Institution of Oceanography, 1997 [available on the Web at <ftp://www.usyd.edu.au/pub/agegrid>].
- [17] H.N. Pollack, S.J. Hurter, J.R. Johnson, Heat flow from the earth's interior: analysis of the global data set, *Rev. Geophys.* 31 (1993) 267–280.
- [18] E.E. Davis, D.S. Chapman, K. Wang, H. Villinger, A.T. Fisher, W. Robinson, J. Grigel, D. Pribnow, J. Stein, K. Becker, Regional heat flow variations across the sedimented Juan de Fuca Ridge eastern flank: Constraints on lithospheric cooling and lateral hydrothermal heat transport, *J. Geophys. Res.* 104 (1999) 17675–17688.
- [19] D.F.C. Pribnow, M. Kinoshita, C.A. Stein, 2000. Thermal data collection and heat flow recalculations for ODP Legs 101–180, Institute for Joint Geoscientific Research, GGA, Hannover, 0120432 [available on the Web at <http://www-odp.tamu.edu/publications/heatflow/>].
- [20] E.E. Davis, K. Wang, J. He, D.S. Chapman, H. Villinger, A. Reseberger, An unequivocal case for high Nusselt number hydrothermal convection in sediment-buried igneous oceanic crust, *Earth Planet. Sci. Lett.* 146 (1997) 137–150.
- [21] K. Wang, J. He, E.E. Davis, Influence of basement topography on hydrothermal circulation in sediment-buried oceanic crust, *Earth Planet. Sci. Lett.* 146 (1997) 151–164.
- [22] M.J. Mottl, C.G. Wheat, Hydrothermal circulation through mid-ocean ridge flanks: fluxes of heat and magnesium, *Geochim. Cosmochim. Acta* 58 (1994) 2225–2237.
- [23] A.T. Fisher, K. Becker, Channelized fluid flow in oceanic crust reconciles heat-flow and permeability data, *Nature* 403 (2000) 71–74.
- [24] A.W. Mantyla, J.L. Reid, Abyssal characteristics of the World Ocean waters, *Deep-Sea Res.* 30 (1983) 805–833.
- [25] H. Elderfield, A. Schultz, Mid-ocean ridge hydrothermal fluxes and the chemical composition of the ocean, *Annu. Rev. Earth Sci.* 24 (1996) 191–224.
- [26] E. Bloechl, R. Rachel, S. Burggraf, D. Hafenbradl, H.W. Jannasch, K.O. Stetter, *Pyrolobus fumarii*, gen. and sp. nov. represents a novel group of archaea, extending the upper temperature limit for life to 113 degrees C, *Extremophiles* 1 (1997) 14–21.
- [27] W.H. Schlesinger, *Biogeochemistry: An Analysis of Global Change*, Academic Press, San Diego, CA, 1997, 574 pp.
- [28] C.G. Wheat, M.J. Mottl, Composition of pore and spring waters from Baby Bare: Global implications of geochemical fluxes from a ridge flank hydrothermal system, *Geochim. Cosmochim. Acta* 64 (2000) 629–642.
- [29] M.J. Pruis, H.P. Johnson, Porosity of very young oceanic crust from sea floor gravity measurements, *Geophys. Res. Lett.* 25 (1998) 1959–1962.

- [30] L.A. Gilbert, H.P. Johnson, Direct measurements of oceanic crustal density at the northern Juan de Fuca Ridge, *Geophys. Res. Lett.* 26 (1999) 3633–3636.
- [31] B.P. Luyendyk, On-bottom gravity profile across the East Pacific Rise crest at 21° North, *Geophysics* 49 (1984) 2166–2177.
- [32] J.R. Cochran, D.J. Fornari, B.J. Coakley, R. Herr, M.A. Tivey, Continuous near-bottom gravity measurements made with a BGM-3 gravimeter in DSV Alvin on the East Pacific Rise crest near 9° 31'N and 9° 50'N, *J. Geophys. Res.* 104 (1999) 10841–10861.
- [33] M.A. Tivey, A. Takeuchi, WMARK Scientific Party, A submersible study of the western intersection of the Mid-Atlantic ridge and Kane fracture zone (WMARK), *Mar. Geophys. Res.* 20 (1998) 195–218.
- [34] J.A. Hildebrand, J.M. Stevenson, P.T.C. Hammer, M.A. Zumberge, R.L. Parker, C.G. Fox, P.J. Meis, A seafloor and sea surface gravity survey of Axial volcano, *J. Geophys. Res.* 95 (B8) (1990) 12751–12763.
- [35] V.S. Ballu, J.A. Hildebrand, S.C. Webb, Seafloor gravity evidence for hydrothermal alteration of the sediments in Middle Valley, Juan de Fuca Ridge, *Mar. Geol.* 150 (1998) 99–111.
- [36] R.L. Evans, A seafloor gravity profile across the TAG hydrothermal mound, *Geophys. Res. Lett.* 23 (1996) 3447–3450.
- [37] J.M. Stevenson, J.A. Hildebrand, Gravity modeling of a volcanically active site on the East Pacific Rise axis, *Tectonophysics* 254 (1996) 57–68.
- [38] J.M. Stevenson, J.A. Hildebrand, M.A. Zumberge, C.G. Fox, An ocean bottom gravity study of the southern Juan de Fuca Ridge, *J. Geophys. Res.* 99 (1994) 4875–4888.
- [39] R.J. Kirkpatrick, Results of downhole geophysical logging hole 396B, *Init. Rep. DSDP 46* (1979) 401–407.
- [40] J. Dubois, C. Deplus, Gravimetry on the Erimo Seamount, Japan, *Tectonophysics* 160 (1989) 267–275.
- [41] D. Goldberg, D. Moos, Physical properties of 110 Ma oceanic crust at site OSN-1: Implications for emplacement of a borehole seismometer, *Geophys. Res. Lett.* 19 (1992) 757–760.
- [42] M.H. Salisbury, T.W. Donnelly, J. Francheteau, Geophysical logging in Deepsea Drilling Project Hole 417D, *Init. Rep. DSDP 51–53 (Part 1)* (1980) 705–713.
- [43] D. Moos, M. Van Schaack, H. Ito, Elastic-wave velocities in Jurassic-age oceanic crust from analysis of sonic full waveform logs in Hole 801C, *Proc. ODP Sci. Results* 144 (1995) 665–671.
- [44] S.M. Wiggins, J.A. Hildebrand, J.M. Geiskes, Geothermal state and fluid flow within ODP Hole 843b: results from wireline logging, *Earth Planet. Sci. Lett.* 195 (2002) 239–248.
- [45] K. Becker et al., Drilling deep into young oceanic crust, Hole 504b, Costa Rica Rift, *Rev. Geophys.* 27 (1989) 79–102.
- [46] M.H. Salisbury, T.W. Donnelly, J. Francheteau, Results of downhole geophysical logging, hole 396B, *DSDP Leg 46, Init. Rep. DSDP 46* (1979) 401–407.